PIER C

Microstrip Antenna with Two Elements and Defected Ground Structure for 5G Mobile Applications at 28/38 GHz

Ekta Thakur[1], Anupma Gupta[1], Muhannad K. Abdulhameed[2,3],
Aymen D. Khaleel[4], and Ahmed Jamal Abdullah Al-Gburi[5,*]

[1]*Department of Interdisciplinary Courses of Engineering, Chitkara Institute of Engineering & Technology*
Chitkara University, Rajpura, Punjab, India
[2]*Computer Scince Department, University of Kerbala, Karbala, Iraq*
[3]*Air Conditioning Engineering Department, Faculty of Engineering, Warith Al-Anbiyaa University, Iraq*
[4]*Computer Engineering Department, College of Engineering, Al-Iraqia University, Iraq*
[5]*Center for Telecommunication Research & Innovation (CeTRI), Faculty of Electronics and Computer Technology and Engineering*
Universiti Teknikal Malaysia Melaka (UTeM), Jalan Hang Tuah Jaya, Durian Tunggal, Melaka 76100, Malaysia

ABSTRACT: A new type of compact line-fed MIMO antenna for 5G wireless communication is presented in this paper. A rectangular microstrip patch antenna with an inset feed is designed for the 28 GHz and 38 GHz bands. T-shaped patch contains inverted I-shaped slots, providing a dual-band response at 28 GHz and 38 GHz. By integrating two T-shaped patches, the MIMO (Multiple Input Multiple Output) antenna significantly improves signal diversity and data throughput, making it highly suitable for modern wireless applications such as 5G networks. Slot-formed defected ground structures (DGSs) are inserted into a partial rectangular ground plane. To fit into handset devices for the upcoming 5G mobile revolution, the antennas are modestly configured on a substrate measuring $14 \times 28 \, \text{mm}^2$, occupying minimal area and reducing mutual coupling. The ECC, MEG, TARC, and radiation efficiency values obtained from the antenna systems are suitable for 5G mobile applications, with excellent reflection coefficient characteristics.

1. INTRODUCTION

Over the past few years, wireless mobile systems with advanced data rates have made substantial developments. The next generation of wireless mobile communication systems will require multiple-input multiple-output (MIMO) technology. Data rate and channel capacity considerably increase as the number of antenna elements increases at both transmission and reception sites. Millimeter-wave frequency bands are likely to be the next generation of mobile communications due to the significant focus of research societies on them today. The frequency ranges used by next-generation wireless systems will include 28 GHz, 38 GHz, 60 GHz, and 73 GHz [1]. Antennas are a crucial component of wireless systems. The path loss of millimeter waves increases with frequency due to atmospheric absorption, making the development of high-gain antennas with compact sizes a significant challenge [2]. The principal design considerations for microstrip antennas in these applications are bandwidth enhancement and size reduction, as improvements in one characteristic often cause declines in the other [3]. Typically, the antenna part of a new RF design must be low profile, low cost, capable of dual or multiple bands, minimally planar, and fit into a small space. Several research projects have been conducted on multiband antenna systems operating at millimeter-wave frequencies [4, 5]. Many designs using multiband techniques are currently being cited

for the use in 5G millimeter wave spectrums. For instance, in [6], the author presents a circular microstrip antenna with an elliptical slot operating at 28 GHz and 45 GHz. A triple-band MIMO antenna with a notch at 5 GHz to block the WiFi channel is described in [7]. An eight-element two-dimensional slot antenna designed for 28 GHz is reported in [8]. An antenna for 28 and 38 GHz and an antenna for 33 GHz with irregular bands are described in [2]. It is shown in [9] that a single-band antenna could enhance the gain at 28 GHz by approximately 15 dB. In [10], two microstrip antenna elements at 28 GHz are implemented on an FR-4 substrate. A concept for designing a multiple antenna array for 28 GHz and 38 GHz for future 5G communications is presented in [11]. An antenna operating at 28 GHz and 38 GHz with a proximity coupling feed slotted is reported in [12]. It is possible to operate a four-element antenna array at 28 GHz, 37 GHz, 41 GHz, and 74 GHz, according to [13]. It is presented in [14] that a massive MIMO antenna would be effective at 28/38 GHz. For upcoming smartphones, eight MIMO elements are designed with dual-band capability, with approximately $7 \times 15.5 \, \text{mm}^2$ of antenna space available for fifth-generation bands. A novel dual-polarized 5G MIMO antenna array [15] for 28 GHz and 38 GHz emphasizes compact design while ensuring efficient performance through dual polarization. The proposed array showcases improved signal quality, interference reduction, and potential for advanced 5G applications in millimeter-wave frequencies.

As proposed in [16], the edges of the triangular antenna recede exponentially as the surface is moved away. The con-

---

* Corresponding author: Ahmed Jamal Abdullah Al-Gburi (ahmedjamal@ieee.org/engahmed_jamall@yahoo.com).

densed surface area of a monopole antenna is typically 10 by 12 millimeters. MIMO antennas with a 2×2 configuration are found to have envelope correlation coefficients of less than 0.001. A cellular smartphone antenna based on millimeter-wave (mm-wave) technology is discussed in this article [17].

This article discusses 5G millimeter wave (5G MW) mobile communication with condensed MIMO antennas. MIMO antennas are manufactured using an inexpensive FR4 substrate (lossy) with $h = 1.6 \, \text{mm}$ and $\varepsilon_r = 4.4$, together with a loss tangent ($\tan \delta = 0.0009$) and dimensions of $w \times L = 14 \times 28 \, \text{mm}^2$. This antenna size is chosen to fit a mobile circuit board approximately the same size as the iPhone SE, with a $14 \, \text{mm} \times 28 \, \text{mm}$ area. The introduced antennas offer several features, including an efficient radiation pattern, matching impedance bandwidths, and dual-band functionality. A MIMO antenna with two ports can achieve isolation greater than 27 dB without any additional components. The compact size of the MIMO antenna allows it to fit within the upper and lower boundaries of contemporary portable gadgets. To facilitate upcoming 5G applications, the triple MIMO antennas have dual-band purposes at 28/38 GHz, according to the simulated results.

2. ANTENNA DESIGN

Antenna is designed using a T-shaped patch with inverted I shaped slots and defected ground surface plane. Detailed design process is evaluated in three steps as shown in Figure 2. Simulation tools HFSS are used to model and predict antenna performance. A physical prototype is then built based on simulation results. Testing the prototype follows, aiming to optimize and refine the antenna design iteratively for improved performance. It consists of two main stages: the one-element antenna design and the MIMO antenna with two symmetrical elements. The resonant effects of multiple antennas can be achieved with planar antenna configurations. The physical dimensions of the antenna are typically determined by the resonant frequency (f_0), dielectric constant (ε_r), and dielectric height (h) using Equations (1) and (2), respectively [18, 19]:

$$Width = \frac{c}{2f_o \sqrt{\frac{\varepsilon_R + 1}{2}}};$$

$$\varepsilon_{eff} = \frac{\varepsilon_R + 1}{2} + \frac{\varepsilon_R - 1}{2} \left[\frac{1}{\sqrt{1 + 12 \left(\frac{h}{W} \right)}} \right] \quad (1)$$

$$Length = \frac{c}{2f_o \sqrt{\varepsilon_{eff}}} - 0.824h \left(\frac{(\varepsilon_{eff} + 0.3) \left(\frac{W}{h} + 0.264 \right)}{(\varepsilon_{eff} - 0.258) \left(\frac{W}{h} + 0.8 \right)} \right) \quad (2)$$

Transformer impedance feedline is considered for port impedance matching with a thin substrate of 1.5 mm thickness. The distance between the feed points in an antenna or transmission line system can significantly affect the input impedance due to changes in the electrical path lengths and the resulting phase differences. As the distance between feed points changes, the impedance seen at the feed point can vary. Proper matching ensures maximum power transfer and minimizes reflections. Secondly, the effective electrical length

of the structure can change with feed point distance, altering the resonant frequency. Thirdly, for antennas, changing feed point distance can affect the current distribution, thereby altering the radiation pattern and potentially affecting gain and directivity. Fourthly, variations in feed point distance can impact the bandwidth over which the system maintains acceptable impedance characteristics. For millimeter-wave 5G mobile communication systems [18], a low-cost, low-profile printed slotted antenna is used. In MIMO designs, the system circuit board size is specified as $14 \, \text{mm} \times 28 \, \text{mm}$, which is appropriate for 5G devices. In photolithography, an antenna model is built by using optical radiation to light a mask on a silicon slab, and then it is measured using Agilent's vector network analyzer N5230C. The radiation pattern is observed in anechoic chambers using microwave shields. A two-element antenna is presented in this section. The 5G mobile application operates at two different frequencies: 28 GHz and 38 GHz. Figure 1 shows the geometrical characteristics of the specified antenna. A 1.6 mm dielectric thickness substrate is used to fabricate the antenna. These patches are made of copper material that radiates from the top and bottom of the substrate.

The concept of mutual coupling [19, 20] is important in the design of multiport antennas because it occurs when two antennas are close to each other. An antenna element's mutual coupling effect is reduced by increasing the distance between them. Grazing lobes are prevented by separating the patch antennas by 10.56 mm. Wide and long inset feeds significantly influence resonance frequencies and return loss levels, so it is crucial to optimize and run many parametric cases to achieve maximum results. For impedance matching and isolation, the backside of the substrate is engraved with a slot. Based on the configured copper solids on the ground plane, Table 1 shows the optimized parameters. Figure 2 shows the equivalent circuit of a two-port inset-fed monopole antenna. The dual-band antenna's equivalent circuit lumped element model includes L_1, R_1, and C_1, which represent the feed line of the antenna. L_2 and C_2 represent the resonant circuit for 28 GHz, and L_3 and C_3 represent the resonant circuit for 38 GHz. L_4 and C_4 represent the mutual coupling between the two monopole antennas.

TABLE 1. Size of the presented antenna.

Parameter	Units (mm)	Parameter	Units (mm)
L_g	28	W_{p1}	1
W_g	14	G_p	13
W_p	6.8	G_{p1}	7.2
Lw	4.5	G_{p2}	0.2
W_w	6.7	L_{p1}	1
W_1	6.6	W_{p2}	2
L_1	9	L_p	3.4

Figure 3(a) illustrates the stepwise expansion of dual-band 5G antenna. It is observed from Figure 3(b) that by inserting inset feed two bands are achieved at 30 GHz and 39 GHz. By inserting I slot in the patch plane dual-band antenna at 28 GHz and 38 GHz is achieved. Figure 4 shows the mutual coupling with and without the Defected Ground Structure (DGS). As ob-
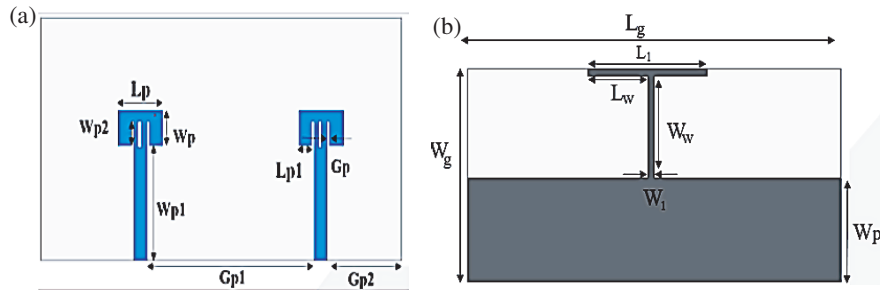
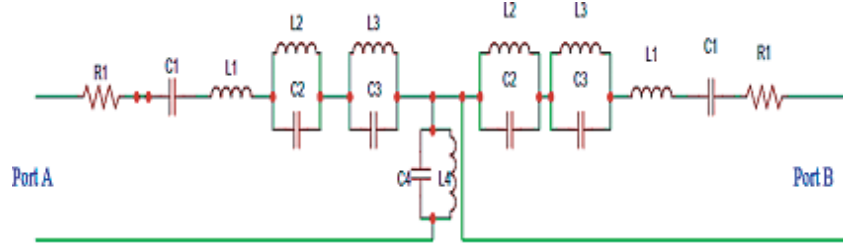**FIGURE 1**. Layout of the designed structure (a) front view, (b) back view.

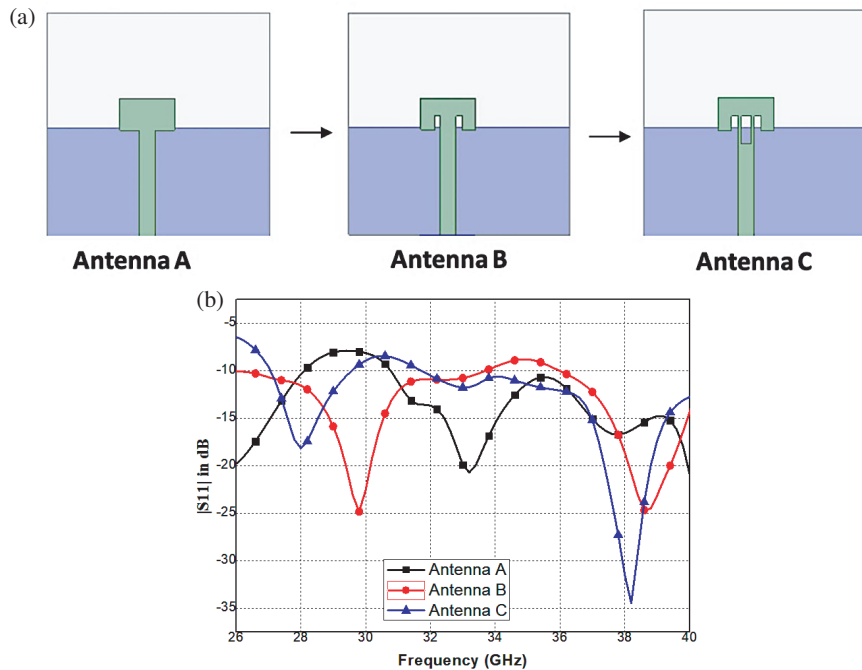**FIGURE 2**. Equivalent circuit Model.

FIGURE 3. (a) Stepwise expansion of Dual band 5G Antenna and (b) reflection coefficient of different 5G Antenna.

served from Figure 3, with DGS, the isolation is improved from -25 dB to -30 dB at 28 GHz and from -20 dB to -25 dB at 38 GHz.

Using high-frequency structure simulator software, the surface current at 28 GHz and 38 GHz is investigated to gain a better understanding of how the introduced antenna functions. The surface current concentrates mainly on the major patches at the resonant frequencies of 28 GHz and 38 GHz, as shown in Figure 5.

3. EXPERIMENTAL RESULTS

The EP 2006 PCB prototype machine is used to create the proposed antenna. Agilent vector network analyzer measures the antenna's scattering properties. In a microwave shielded anechoic chamber, the antenna's gain and radiation pattern are monitored. Figure 6 illustrates the fabricated T-shaped 5G MIMO antenna configuration. At 28 GHz and 38 GHz, the two systems resonate, and the reflection coefficient plot is shown in Figure 7. To enhance the isolation, a square slot and an
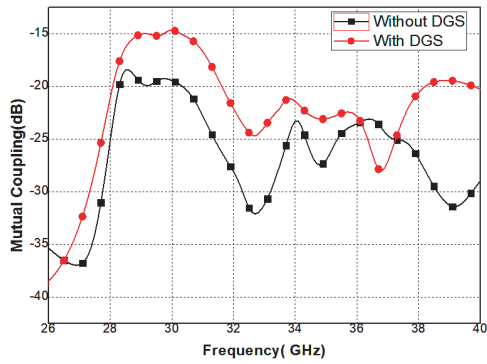
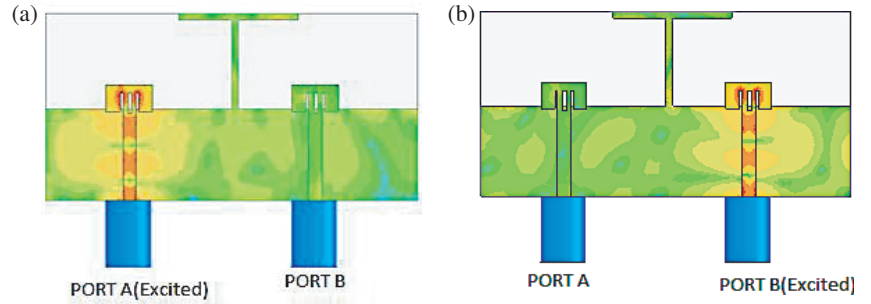FIGURE 4. Mutual coupling with and without DGS.

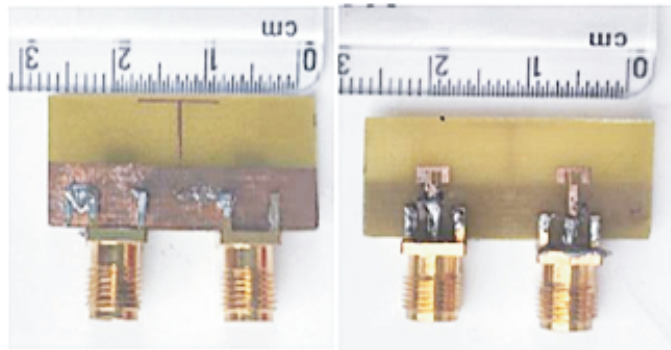FIGURE 5. Surface current distribution on suggested antenna.
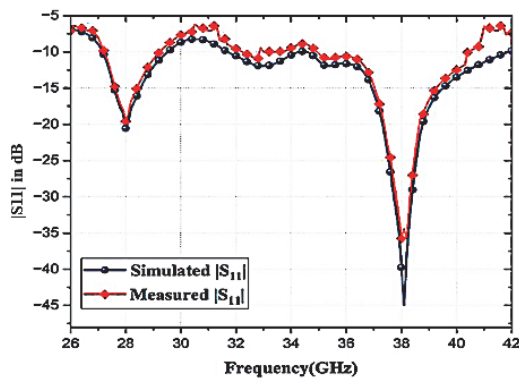

FIGURE 6. Fabricated Antenna.
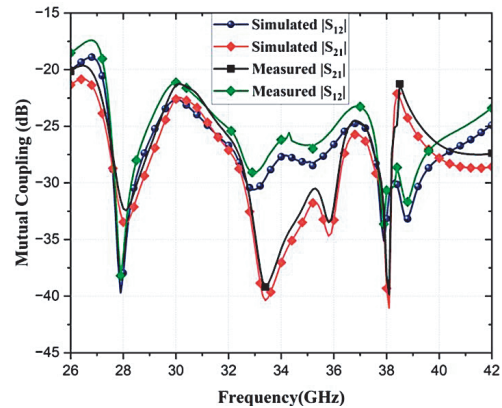

FIGURE 7. Reflection coefficient plot.

FIGURE 8. Measured and simulated mutual coupling.

inverse L-shaped strip are etched and coupled with a ground plane. Simulated results are achieved using the software program Ansoft HFSS v.13.

The return loss of the antenna suggested in Figure 4 has been simulated and tested. In this model, W_{p1}, W_p, W_{p2}, L_P, G_p, and L_{P1} are parametrically tuned to achieve two frequency bands of 28 GHz and 38 GHz. In 5G wireless communication, both of these bands are used. For the two-port antenna system shown in Figure 8, mutual coupling is illustrated. Since both antennas operate independently at 28 GHz and 38 GHz mm-wave frequencies, their mutual coupling value is very low. Measurement and simulation results match reasonably well.

The simulated and tested results can differ depending on various factors, including manufacturing tolerances, the loss tangent of FR4, mismatches between antenna feeds and connections, connector loss, and inadequate soldering [21–24].

3.1. MIMO Diversity Performance

MIMO antennas with two elements are used to increase data throughput [25–28]. A MIMO antenna has very close spacing between its antenna elements, presenting a challenging design issue. This results in increased port coupling and field coupling. Channel capacity [29] and antenna efficiency are impacted by these couplings. High port isolation and low correla-
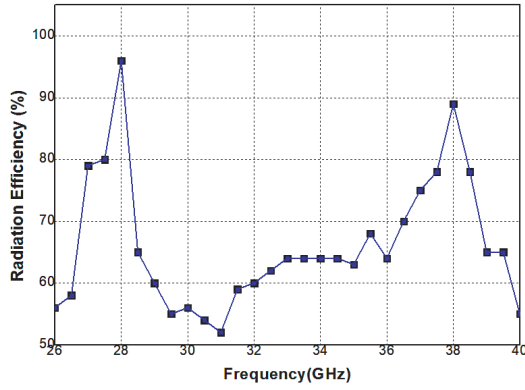
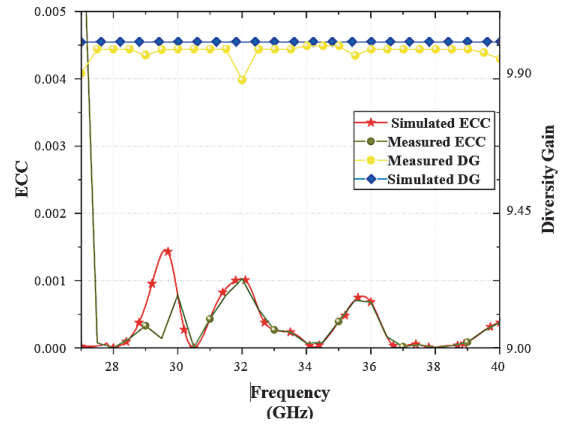FIGURE 9. Radiation Efficiency of suggested antenna.
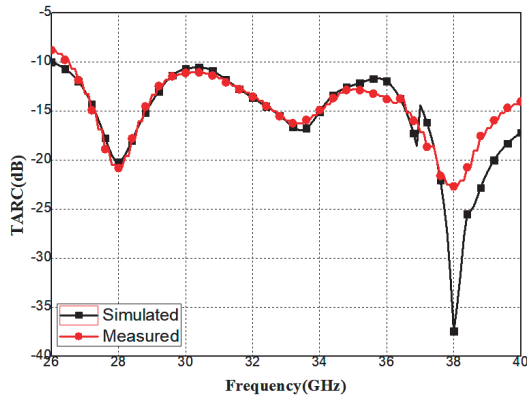

FIGURE 10. Measured and simulated ECC and DG.

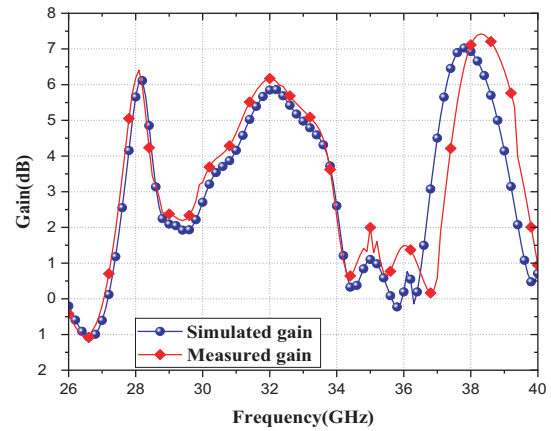FIGURE 11. Measured and simulated TARC.

FIGURE 12. Gain of the presented antenna.

tion levels are essential. MIMO antennas have a variety of performance characteristics, including Envelope Correlation Coefficients (ECC), Diversity Gains (DGs), and Total Active Reflection Coefficients (TARCs). Radiation patterns between two radiating MIMO elements can be estimated using the ECC [30].

Figure 9 shows the radiation efficiency of the suggested antenna. The achieved efficiency at 28 GHz is 96% and at 38 GHz is 90%. Using a two-port antenna system [29], the ECC [29] and TARC [29] can be obtained as follows:

$$ECC = \frac{\left|S_{11}^* S_{12} + S_{21}^* S_{22}\right|^2}{\left(1 - |S_{11}| - |S_{12}|\right)^2 \left(1 - |S_{21}| - |S_{22}|\right)^2} \quad (3)$$

$$TARC = \sqrt{\frac{\left(S_{11} + S_{12}\right)^2 + \left(S_{21} + S_{22}\right)^2}{2}} \quad (4)$$

where S_{11}, S_{22}, S_{12}, and S_{21} are the S parameters of the scattering matrix. In Figure 10, satisfactory ECC values are shown for the operating band. For multi-port antenna systems, TARC [30] must be evaluated since the reflection coefficient is considered only for single-element antennas [28, 30–36].

In Figure 11, satisfactory TARC values are shown for the operating band, and in Figure 8, the DG is around 9.99 dB. A very low ECC value can be achieved for the entire resonating band

due to the polarization diversity of the proposed antenna system. In addition to the gain, the antenna's ability to transmit and receive electromagnetic waves is also greatly affected by the direction in which it transmits [43, 44]. An illustration of the variation of gain with frequency can be seen in Figure 12. It is also important to consider the gain when describing the antenna's capability to transmit and receive electromagnetic waves. The peak gain measured at 28 GHz and 38 GHz are 6.2 and 7 dBi. The radiation patterns are shown in Figure 13 in both the E- and H-planes for all three stages of antenna evolution 3(a) and (b), respectively. It is seen that the antenna elements emit equally for both planes at both operating frequencies.

Another performance statistic, DG, is used to illustrate how much transmission power has been reduced. It is calculated from the ECC using the following calculation [37–42].

$$DG = \sqrt{1 - |ECC|^2} \quad (5)$$

3.2. Specific Absorption Rate (SAR)

Specific absorption rate of the proposed structure on a numerical muscle equivalent phantom is shown in Figure 14. to the safety standards, IEEE C95.1-1999 SAR is restricted to 2.0 W/Kg over 10 grams of body tissue. For the designed structure SAR is 1.85 W/Kg for the 28 GHz frequency and
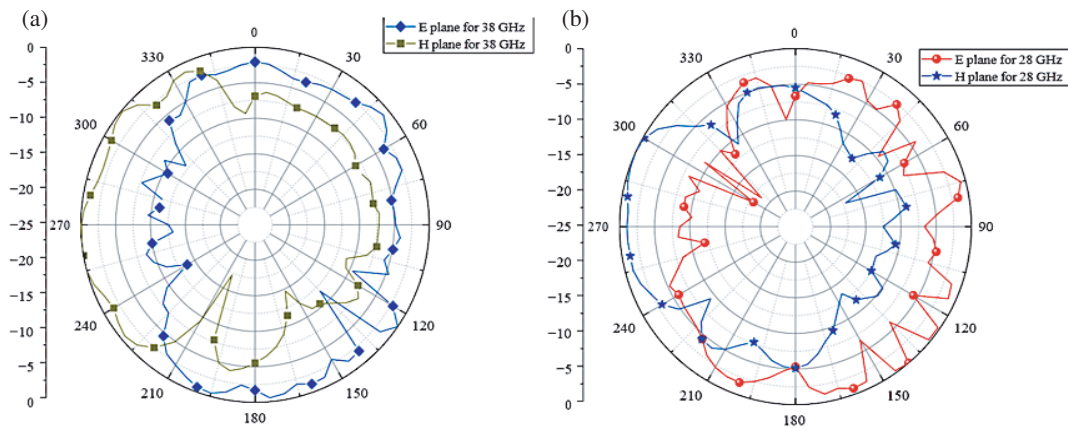
FIGURE 13. Suggested antenna's radiation plot for both frequencies (a) 38 GHz and (b) 28 GHz.
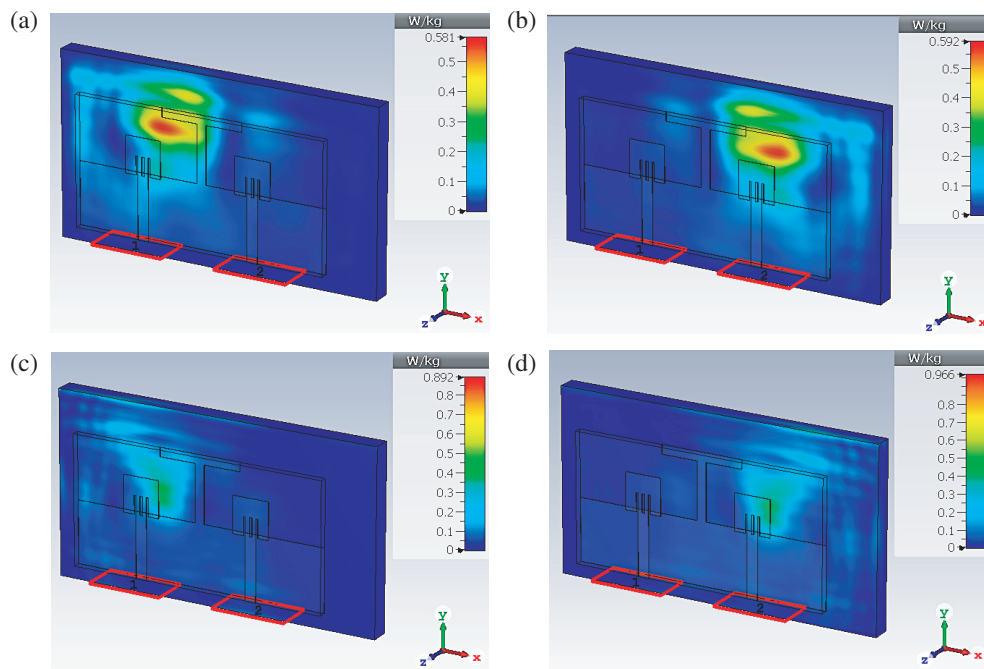

FIGURE 14. Specific absorption rate (a) at 28 GHz port1, (b) at 28 GHz port2, (c) at 38 GHz port1, (d) at 38 GHz port2.

TABLE 2. SAR for 15 dBm input power.

Frequency (GHz)	SAR (W/kg.)	Frequency (GHz)	SAR (W/kg.)
28 GHz (port1)	1.31	38 GHz (port1)	2.0
28 GHz (port2)	1.34	38 GHz (port2)	2.1

0.892 W/Kg for the 38 GHz frequency at the applied input power of 0.1 mW at a distance of 5 mm from antenna. According to Federal Communications Commission (FCC) input power for 5G systems can be set to 15 dBm, 18 dBm, and 20 dBm [45]. Table 2 indicates that as the frequency increases from 28 GHz to 38 GHz, the SAR values also increase, suggesting a higher absorption of power in the tissue at the higher frequency. This trend is consistent across both ports. The dif-

ference in SAR values between the two ports at each frequency is minimal, indicating a similar distribution of power absorption in the tissue for both ports.

A comparison of the suggested MIMO antenna with recently published 5G MIMO antennas in the literature is shown in Table 2. The performance of the MIMO antenna (ECC, DG, and TARC) is examined along with antenna size, operating frequency, maximum mutual coupling, gain, and other features

TABLE 3. Comparative study of different 5G MIMO antenna.

Reference	Dimensions mm^3	Mutual coupling	Resonant frequency (GHz)	Gain (dB)	ECC	DG
[46]	$(95 \times 49.7 \times 21.6)$	-26	3.3–3.8	4.83	0.03	9.8
[47]	$(80 \times 80 \times 12)$	-15.5	3.08–7.75	8	0.04	9.98
[48]	$(70 \times 40 \times 7.048)$	-25	4.2–4.9	NA	0.001	9.9
[49]	$(20 \times 40 \times 1.6)$	-29.34	28 GHz	7	0.005	9.95
[50]	$(28 \times 16 \times 6.3)$	-33	40	10	0.1	9.98
[51]	$(26 \times 14.5 \times 0.508)$	-39 at 28 GHz and -39 at 38 GHz	Dual-band 28 and 38 GHz	5.2 at 28 GHz and 5.5 at 28 GHz	0.001	9.98
[52]	NA	-35 GHz	4.95 GHz	10.6	NA	NA
[53]	NA	-35 GHz	10 GHz	13.5	NA	NA
Suggested Antenna	$(28 \times 14 \times 1.6)$	-40 at 28 GHz and -42 at 38 GHz	Dual-band 28 and 38 GHz	6.2 at 28 GHz and 7 at 38 GHz	0.0015	9.99

of the antenna design. A few studies have reportedly discussed reducing mutual coupling by employing defected ground structures. A diversity MIMO system with improved isolation based on decoupling structures was presented by the authors in [46–53] and recorded in Table 3. It has been demonstrated that the designed MIMO antenna achieves maximum isolation at the two resonant frequencies. Additionally, despite having a low profile and small structure, it provides remarkable diversity performance. Although a few studies showed greater improvements, the complexity and size increased.

4. CONCLUSION

A MIMO antenna with two resonant millimeter-wave bands and minimal isolation is suggested to meet the high-performance requirements of the 5G MIMO communication system. A small monopole radiating antenna is chosen to produce a two-band response at 28/38 GHz. The MIMO system, which uses two radiating components placed next to one another, measures $28 \times 14 \times 1.6$ mm^3. To improve mutual coupling at both frequencies without altering the system's footprint, a defected ground plane is built and placed between the two MIMO components. To achieve remarkable performance at millimeter waves, the radiating components are placed on a low-loss FR4 substrate. According to the simulated and measured results, the 5G MIMO antennas have dual-band functionality at 28/38 GHz to facilitate upcoming 5G applications.

ACKNOWLEDGEMENT

REFERENCES

[1] Sharma, M., "Microstrip biomedical patch antenna with MIMO capability and challenges in achieving diversity performance," in *Internet of Things Enabled Antennas for Biomedical Devices and Systems*, P. K. Malik and P. N. Shastry (eds.), Springer Tracts in Electrical and Electronics Engineering, Springer, Singapore, 2023.

[2] Elabd, R. H. and A. J. A. Al-Gburi, "Ultra-compact 4-port MIMO antenna with defected ground structure and SAR analysis for 28/38 GHz 5G mobile devices," *Journal of Electromagnetic Waves and Applications*, Vol. 38, No. 9, 1000–1025, 2024.

[3] Abdullah Al-Gburi, A. J., "5G MIMO antenna: Compact design at 28/38 GHz with metamaterial and SAR analysis for mobile phones," *Przeglad Elektrotechniczny*, Vol. 2024, No. 4, 171–174, 2024.

[4] Ren, W., Z. Wang, W. Nie, W. Mu, C. Li, M. Wang, and W. You, "A 12-unit asymmetric mirror-coupled loop antenna for 5G smartphones," *Progress In Electromagnetics Research C*, Vol. 145, 141–152, 2024.

[5] Kumar, P., A. K. Singh, R. Kumar, S. K. Mahto, P. Pal, R. Sinha, A. Choubey, and A. J. A. Al-Gburi, "Design and analysis of low profile stepped feedline with dual circular patch MIMO antenna and stub loaded partial ground plane for wireless applications," *Progress In Electromagnetics Research C*, Vol. 140, 135–144, 2024.

[6] Kumar, G. K., "A survey on planar ultra-wideband antennas with band notch characteristics: Principle, design, and applications," *AEU — International Journal of Electronics and Communications*, Vol. 109, 76–98, 2019.

[7] Farahat, A. E. and K. F. A. Hussein, "28/38 GHz dual-band Yagi-Uda antenna with corrugated radiator and enhanced reflectors for 5G MIMO antenna systems," *Progress In Electromagnetics Research C*, Vol. 101, 159–172, 2020.

[8] Kumar, S. and A. Kumar, "Design of circular patch antennas for 5G applications," in *2019 2nd International Conference on Innovations in Electronics, Signal Processing and Communication (IESC)*, 287–289, Shillong, India, 2019.

[9] Elsharkawy, R. R., K. F. A. Hussein, and A. E. Farahat, "Dual-band (28/38 GHz) compact MIMO antenna system for millimeter-wave applications," *Journal of Infrared, Millimeter, and Terahertz Waves*, Vol. 44, No. 11, 1016–1037, 2023.

[10] Ahmad, W. and W. T. Khan, "Small form factor dual band (28/38 GHz) PIFA antenna for 5G applications," in *2017 IEEE MTT-S International Conference on Microwaves For Intelligent Mobility (ICMIM)*, 21–24, Nagoya, Japan, 2017.

[11] He, Y., M. Rao, Y. Liu, G. Jing, M. Xi, and L. Zhao, "28/39-GHz dual-band dual-polarized millimeter wave stacked patch antenna array for 5G applications," in *2020 International Workshop on Antenna Technology (iWAT)*, 1–4, Bucharest, Romania, 2020.

[12] Farahat, A. E. and K. F. A. Hussein, "Dual-band (28/38 GHz) wideband MIMO antenna for 5G mobile applications," *IEEE Access*, Vol. 10, 32 213–32 223, 2022.

[13] Sharma, M., P. C. Vashist, I. Alsukayti, N. Goyal, D. Anand, and A. H. Mosavi, "A wider impedance bandwidth dual filter symmetrical MIMO antenna for high-speed wideband wireless applications," *Symmetry*, Vol. 14, No. 1, 29, 2021.

[14] Goyal, R. K. and U. S. Modani, "A compact microstrip patch antenna at 28 GHz for 5G wireless applications," in *2018 3rd International Conference and Workshops on Recent Advances and Innovations in Engineering (ICRAIE)*, 1–2, Jaipur, India, 2018.

[15] Cuneray, K., N. Akcam, T. Okan, and G. O. Arican, "28/38 GHz dual-band MIMO antenna with wideband and high gain properties for 5G applications," *AEU — International Journal of Electronics and Communications*, Vol. 162, 154553, 2023.

[16] Khan, D., A. Ahmad, and D.-Y. Choi, "Dual-band 5G MIMO antenna with enhanced coupling reduction using metamaterials," *Scientific Reports*, Vol. 14, No. 1, 96, 2024.

[17] Tiwari, R. N., D. Sharma, P. Singh, and P. Kumar, "A flexible dual-band 4 × 4 MIMO antenna for 5G mm-wave 28/38 GHz wearable applications," *Scientific Reports*, Vol. 14, No. 1, 14324, 2024.

[18] Thakur, V., N. Jaglan, and S. D. Gupta, "Design of a dual-band 12-element MIMO antenna array for 5G mobile applications," *Progress In Electromagnetics Research Letters*, Vol. 95, 73–81, 2021.

[19] Elabd, R. H. and A. J. A. Al-Gburi, "Low mutual coupling miniaturized dual-band quad-port MIMO antenna array using decoupling structure for 5G smartphones," *Discover Applied Sciences*, Vol. 6, No. 4, 189, 2024.

[20] Kumar, P., A. K. Singh, R. Kumar, R. Sinha, S. K. Mahto, A. Choubey, and A. J. A. Al-Gburi, "High isolated defected ground structure based elliptical shape dual element MIMO antenna for S-band applications," *Progress In Electromagnetics Research C*, Vol. 143, 67–74, 2024.

[21] Liu, P., Y. Sun, T. Liu, Q. Li, and X. Wang, "Wideband 10-port MIMO antenna array for 5G metal-frame smartphone applications," *Progress In Electromagnetics Research C*, Vol. 104, 229–240, 2020.

[22] Parchin, N. O., H. J. Basherlou, Y. I. A. Al-Yasir, and R. A. Abd-Alhameed, "A design of antenna array with improved performance for future smartphones," *Progress In Electromagnetics Research C*, Vol. 101, 1–12, 2020.

[23] Aziz, H. S. and D. K. Naji, "Printed 5G MIMO antenna arrays in smartphone handset for lte bands 42/43/46 applications," *Progress In Electromagnetics Research M*, Vol. 90, 167–184, 2020.

[24] Pandya, K., T. Upadhyaya, U. Patel, V. Sorathiya, A. Pandya, A. J. A. Al-Gburi, and M. M. Ismail, "Performance analysis of quad-port UWB MIMO antenna system for sub-6 GHz 5G, WLAN and X band communications," *Results in Engineering*, Vol. 22, 102318, 2024.

[25] Wei, G. and Q. Feng, "Dual-band MIMO antenna array for compact 5G smartphones," *Progress In Electromagnetics Research C*, Vol. 99, 157–165, 2020.

[26] Karthikeya, G. S., M. P. Abegaonkar, and S. K. Koul, "A wideband conformal antenna with high pattern integrity for mmwave 5G smartphones," *Progress In Electromagnetics Research Letters*, Vol. 84, 1–6, 2019.

[27] El-Hassan, M. A., A. E. Farahat, and K. F. A. Hussein, "Quad-band MIMO antenna system for 5G mobile handsets," *The Applied Computational Electromagnetics Society Journal (ACES)*, Vol. 36, No. 11, 1418–1428, 2021.

[28] El Halaoui, M., L. Canale, A. Asselman, and G. Zissis, "Dual-band 28/38 GHz inverted-F array antenna for fifth generation mobile applications," in *Proceedings of the 14th International Conference on Interdisciplinarity in Engineering — INTER-ENG 2020*, Vol. 63, No. 1, 53, Targu Mures, Romania, 2020.

[29] Farahat, A. E. and K. F. A. Hussein, "Dual-band (28/38 GHz) wideband MIMO antenna for 5G mobile applications," *IEEE Access*, Vol. 10, 32 213–32 223, 2022.

[30] Elabd, R. H. and A. J. A. Al-Gburi, "SAR assessment of miniaturized wideband MIMO antenna structure for millimeter wave 5G smartphones," *Microelectronic Engineering*, Vol. 282, 112098, 2023.

[31] Elabd, R. H. and A. J. A. Al-Gburi, "Super-compact 28/38 GHz 4-port MIMO antenna using metamaterial-inspired ebg structure with SAR analysis for 5G cellular devices," *Journal of Infrared, Millimeter, and Terahertz Waves*, Vol. 45, No. 1, 35–65, 2024.

[32] Kalyani, G., K. J. Babu, and R. Madhu, "A novel compact two-port MIMO antenna verified with tcm analysis for 28/38 GHz 5G mm-wave applications," in *2024 IEEE Wireless Antenna and Microwave Symposium (WAMS)*, 1–5, Visakhapatnam, India, 2024.

[33] Karthikeya, G. S., M. P. Abegaonkar, and S. K. Koul, "A wideband conformal antenna with high pattern integrity for mmWave 5G smartphones," *Progress In Electromagnetics Research Letters*, Vol. 84, 1–6, 2019.

[34] Mishra, P., M. P. Singh, A. Sharma, K. V. Srivastava, and S. Ghosh, "A dual-band millimeter wave SRR loaded printed monopole with annular slot MIMO antenna for 5G applications," in *2022 52nd European Microwave Conference (EuMC)*, 552–555, Milan, Italy, 2022.

[35] Wei, F., L. Chen, X.-W. Shi, and C.-J. Gao, "UWB bandpass filter with one tunable notch-band based on DGS," *Journal of Electromagnetic Waves and Applications*, Vol. 26, No. 5–6, 673–680, 2012.

[36] Jetti, C. R., T. Addepalli, S. R. Devireddy, G. K. Tanimki, A. J. A. Al-Gburi, Z. Zakaria, and P. Sunitha, "Design and analysis of modified U-shaped four element MIMO antenna for dual-band 5G millimeter wave applications," *Micromachines*, Vol. 14, No. 8, 1545, 2023.

[37] Thakur, E., N. Jaglan, A. Gupta, and A. J. A. Al-Gburi, "Multi-band notched circular polarized mimo antenna for ultrawideband applications," *Progress In Electromagnetics Research M*, Vol. 125, 87–95, 2024.

[38] Ali, A., M. E. Munir, M. M. Nasralla, M. A. Esmail, A. J. A. Al-Gburi, and F. A. Bhatti, "Design process of a compact tri-band MIMO antenna with wideband characteristics for sub-6 GHz, Ku-band, and millimeter-wave applications," *Ain Shams Engineering Journal*, Vol. 15, No. 3, 102579, 2024.

[39] Zeain, M. Y., M. Abu, A. A. Althuwayb, H. Alsariera, A. J. A. Al-Gburi, A. A. Abdulbari, and Z. Zakaria, "A new technique of FSS-based novel chair-shaped compact MIMO antenna to enhance the gain for sub-6 GHz 5G applications," *IEEE Access*, Vol. 12, 49 489–49 507, 2024.

[40] Rahul, C., S. Debdeep, G. Debarati, S. Chinmoy, J. Y. Siddiqui, and Y. M. M. Antar, "Four element MIMO antenna system based on SRR loaded printed monopoles for 28/38 GHz 5G applica-

tions," in *2020 International Symposium on Antennas & Propagation (APSYM)*, 36–39, Cochin, India, 2020.

[41] Gomez-Villanueva, R., R. Linares-y Miranda, J. A. Tirado-Mendez, and H. Jardon-Aguilar, "Ultra-wideband planar inverted-f antenna (PIFA) for mobile phone frequencies and ultra-wideband applications," *Progress In Electromagnetics Research C*, Vol. 43, 109–120, 2013.

[42] Liu, G., J. Gu, Z. Gao, T. Tang, and X. Zhang, "Hexa-band mobile antenna with FSS-R-Card combination for SAR reduction," *Progress In Electromagnetics Research Letters*, Vol. 114, 83–89, 2023.

[43] Farooq, N., K. Muzaffar, and S. A. Malik, "Compact elliptical slot millimeter-wave MIMO antenna for 5G applications," *Journal of Infrared, Millimeter, and Terahertz Waves*, 1–24, 2024.

[44] Wei, F., X. Liu, X.-Z. Ding, X.-B. Zhao, and P.-Y. Qin, "A balanced filtering antenna array with high gain, steep selectivity, and multi-radiation nulls parallel-fed by differential broadband network," *IEEE Transactions on Antennas and Propagation*, Vol. 71, No. 12, 9926–9931, 2023.

[45] Chen, H. N., J.-M. Song, and J.-D. Park, "A compact circularly polarized MIMO dielectric resonator antenna over electromagnetic band-gap surface for 5G applications," *IEEE Access*, Vol. 7, 140 889–140 898, 2019.

[46] Lak, A., Z. Adelpour, H. Oraizi, and N. Parhizgar, "Design and SAR assessment of three compact 5G antenna arrays," *Scientific Reports*, Vol. 11, No. 1, 21265, 2021.

[47] Hasan, M. M., M. T. Islam, M. Samsuzzaman, M. H. Baharuddin, M. S. Soliman, A. Alzamil, I. I. M. A. Sulayman, and M. S. Islam, "Gain and isolation enhancement of a wideband MIMO antenna using metasurface for 5G sub-6 GHz communication systems," *Scientific Reports*, Vol. 12, No. 1, 9433, 2022.

[48] Wang, M., F. Li, Y. Li, and X. Jing, "A high isolation dual-polarized antenna array with coplanar parasitic decoupling wall," *AEU — International Journal of Electronics and Communications*, Vol. 150, 154203, 2022.

[49] Park, J.-D., M. Rahman, and H. N. Chen, "Isolation enhancement of wide-band MIMO array antennas utilizing resistive loading," *IEEE Access*, Vol. 7, 81 020–81 026, 2019.

[50] Khajeh-Khalili, F., M. A. Honarvar, M. Naser-Moghadasi, and M. Dolatshahi, "Gain enhancement and mutual coupling reduction of multiple-intput multiple-output antenna for millimeter-wave applications using two types of novel metamaterial structures," *International Journal of RF and Microwave Computer-aided Engineering*, Vol. 30, No. 1, e22006, 2020.

[51] Esmail, B. A. and S. Koziel, "High isolation metamaterial-based dual-band MIMO antenna for 5G millimeter-wave applications," *AEU — International Journal of Electronics and Communications*, Vol. 158, 154470, 2023.

[52] Diman, A. A., F. Karami, P. Rezaei, A. Amn-E-Elahi, Z. Mousavirazi, T. A. Denidni, and A. A. Kishk, "Efficient SIW-feed network suppressing mutual coupling of slot antenna array," *IEEE Transactions on Antennas and Propagation*, Vol. 69, No. 9, 6058–6063, 2021.

[53] Nimehvari Varcheh, H. and P. Rezaei, "Integration of the modified butler matrix and decoupling network for beam-steering antenna array," *International Journal of RF and Microwave Computer-Aided Engineering*, Vol. 32, No. 3, e23015, 2022.